Black Hole Formation in Randall-Sundrum II Braneworlds

Daoyan Wang[1] and Matthew W. Choptuik[2,3]
[1]6282 Kathleen Avenue, Suite 204, Burnaby, British Columbia, V5H 4J4 Canada
[2]Department of Physics and Astronomy, University of British Columbia, Vancouver, British Columbia, V6T 1Z1 Canada
[3]CIFAR Cosmology and Gravity Program, 180 Dundas St W, Suite 1400, Toronto, Ontario, Canada M5G 1Z8
(Received 18 April 2016; published 1 July 2016)

We present the first numerical study of the full dynamics of a braneworld scenario, working within the framework of the single brane model of Randall and Sundrum. In particular, we study the process of gravitational collapse driven by a massless scalar field which is confined to the brane. Imposing spherical symmetry on the brane, we show that the evolutions of sufficiently strong initial configurations of the scalar field result in black holes that have finite extension into the bulk. Furthermore, we find preliminary evidence that the black holes generated form a unique sequence, irrespective of the details of the initial data. The black hole solutions we obtain from dynamical evolutions are consistent with those previously computed from a static vacuum ansatz.

DOI: 10.1103/PhysRevLett.117.011102

Introduction.—The basic idea of braneworld scenarios is that our observable Universe could be a $(3+1)$-dimensional brane embedded in a higher-dimensional bulk spacetime. The second such model invented by Randall and Sundrum, known as RSII, is a $(4+1)$-dimensional braneworld containing a single brane on which all matter is confined and one extra dimension of infinite size into which only gravity can propagate [1]. This model is remarkable for its simplicity and recovers general relativity (GR) on the brane in the weak field regime [2] even though the extra dimension is of infinite extent. However, the behavior of the model in the context of strong, dynamical gravitational fields is not as clear and is the focus of this Letter.

One vacuum solution of the RSII model is [1,3]

$$ds^2 = \frac{\ell^2}{z^2}(h_{ab}dx^a dx^b + dz^2), \quad \text{where } z \geq \ell. \qquad (1)$$

Here, z labels the extra dimension, with the single brane of the RSII model located at $z = \ell$, h_{ab} is the metric of a Ricci-flat solution to Einstein's equations in four dimensions [3], and x^a, $a = 0, 1, 2, 3$ are the coordinates on the brane. When h_{ab} is the Minkowski metric, the spacetime described by Eq. (1) is a part of a Poincaré patch of an anti–de Sitter (AdS) spacetime with AdS length ℓ [4]. When h_{ab} is a four-dimensional black hole metric, Eq. (1) describes a black string [3]. However, due to the Gregory-Laflamme instability [5], we do not expect that black strings will form from generic gravitational collapse of matter on the brane and a natural question that arises is, what are the end states of such collapse processes?

Noting that the Gregory-Laflamme instability is most severe at the AdS horizon where black strings might "pinch-off," Chamblin, Hawking, and Reall proposed that collapse would yield a black object with finite extension into the bulk, i.e., a black hole [3]. Many groups have since investigated one aspect of the Chamblin-Hawking-Reall proposal—the existence of such black holes—using both analytical and numerical approaches (see Ref. [6] and references therein). One issue that became a key topic of debate in these studies was whether or not black holes with sizes large relative to the AdS scale ℓ could even exist. Eventually, Figueras and Wiseman [6] obtained black holes with sizes in the approximate range $[0.07\ell, 20\ell]$ (then $\sim[5\times10^{-4}\ell, 100\ell]$ in Ref. [7]) by numerically constructing the solutions of static vacuum RSII spacetimes. Their technique involved perturbing $\mathrm{AdS}_5/\mathrm{CFT}_4$ solutions, which themselves were numerically constructed [8]. Additionally, black holes, including ones with large sizes, were obtained numerically by Abdolrahimi *et al.* [9]. Although they used a different computational approach than Figueras and Wiseman, they also assumed that the spacetimes were static and vacuum, and the two sets of results are presumably consistent.

Without proving the stability and uniqueness of these solutions, however, it is not clear whether they describe the end states of matter collapse on the brane. A direct way to address this and other issues is to solve numerically the full set of dynamical Einstein-matter equations for a simple collapse process, and this is what is described in the remainder of this Letter. To our knowledge, this is the first numerical work that treats the full dynamics of a braneworld scenario with physical branes. Because of the prohibitive computational cost of performing the calculations in the fully five-dimensional context, we start with one of the simplest possible setups in which a black hole could form. This involves (a) imposing spherical symmetry on the brane, which makes the bulk axisymmetric, and (b) using a massless scalar field as the matter source confined on the brane.

Methodology.—For convenience, we define the "background" spacetime as that described by Eq. (1) with h_{ab}

being the Minkowski metric. We study gravitational collapse in the RSII spacetimes that asymptotically go to this background at all spatial infinities. It is known that Cauchy surfaces exist in the RSII spacetimes [3], and the evolution can thus be formulated as an initial value problem with Einstein's equations in the bulk providing the governing equations for the gravitational field. On the brane the scalar field satisfies its usual $3+1$ equation of motion. Additionally, the brane and the matter confined to it are coupled to the bulk through Israel's junction conditions [10]. We use coordinates (t, r, θ, ϕ, z) adapted to the axisymmetry in the bulk: once spherical symmetry on the brane is imposed, the coordinate system is effectively cylindrical, with dynamical variables depending on (t, r, z), and we thus refer to it as such. The numerical calculations are carried out using finite difference approximation and employ coordinates $\hat{R} = r/(r + r_0)$ and $\hat{Z} = (z - \ell)/(z - \ell + z_0)$, where r_0 and z_0 are adjustable parameters, which compactify the spatial domain. We adopt the generalized harmonic formalism of GR [11], which yields a strongly hyperbolic set of evolution equations and, correspondingly, a well-posed initial value problem.

To utilize existing numerical relativity techniques regarding coordinate choices, which have typically been applied only to asymptotically flat spacetimes, we perform a conformal transformation so that the conformally transformed spacetimes are asymptotically flat. Denoting the metric of the physical spacetime as $g_{\mu\nu}$, the conformally transformed metric is defined as $\tilde{g}_{\mu\nu} \equiv \Psi^{-2} g_{\mu\nu}$, where the conformal function Ψ goes to ℓ/z at spatial infinity. Under the conformal transformation the field equations have the form of Einstein's equations in terms of $\tilde{g}_{\mu\nu}$, with an additional term related to Ψ [12] that can be treated as a matter contribution, from the perspective of $\tilde{g}_{\mu\nu}$.

Because of our use of cylindrical coordinates, we must exercise care to minimize irregularities in the numerical solutions at and near the axis of symmetry. Our approach is to first carry the Cartesian components of the various tensors and pseudotensors appearing in our scheme into cylindrical coordinates via coordinate transformation relations. We then let these components serve as fundamental dynamical variables in the numerical calculations. The interested reader is directed to Ref. [13] for a complete description of this methodology, as well as many other additional details of the calculations. In terms of such components, the most generic form of the metric in axisymmetry can be written as

$$\tilde{g}_{\alpha\beta} = \begin{pmatrix} \tilde{\eta}_{tt} & \tilde{\eta}_{tr} & 0 & 0 & \tilde{\eta}_{tz} \\ \tilde{\eta}_{tr} & \tilde{\eta}_{rr} & 0 & 0 & \tilde{\eta}_{rz} \\ 0 & 0 & \tilde{\eta}_{\theta\theta} r^2 & 0 & 0 \\ 0 & 0 & 0 & \tilde{\eta}_{\theta\theta} r^2 \sin^2\theta & 0 \\ \tilde{\eta}_{tz} & \tilde{\eta}_{rz} & 0 & 0 & \tilde{\eta}_{zz} \end{pmatrix}. \quad (2)$$

The boundary conditions at the symmetry axis ($r = 0$) are $\tilde{\eta}_{tt,r} = \tilde{\eta}_{rr,r} = \tilde{\eta}_{zz,r} = \tilde{\eta}_{tz,r} = \tilde{\eta}_{tr} = \tilde{\eta}_{rz} = 0$. The metric function $\tilde{\eta}_{\theta\theta}$ is rewritten as $\tilde{\eta}_{rr} + r\tilde{W}$, so that the local flatness condition [13,14] $\tilde{\eta}_{\theta\theta}|_{r=0} = \tilde{\eta}_{rr}|_{r=0}$ is automatically satisfied. The parity condition $\tilde{\eta}_{\theta\theta,r}|_{r=0} = 0$ then becomes $W|_{r=0} = 0$. Similarly to Eq. (2), the source functions of the generalized harmonic formalism, $\tilde{H}_\mu = -\tilde{g}_{\mu\nu}\tilde{\Gamma}^\nu_{\alpha\beta}\tilde{g}^{\alpha\beta}$, are expressed in terms of Cartesian components $\tilde{h}_\mu$ as

$$\begin{pmatrix} \tilde{H}_t \\ \tilde{H}_r \\ \tilde{H}_\theta \\ \tilde{H}_\phi \\ \tilde{H}_z \end{pmatrix} = \begin{pmatrix} \tilde{h}_t + (2/r)(\tilde{\eta}_{tr}/\tilde{\eta}_{\theta\theta}) \\ \tilde{h}_r + (2/r)(\tilde{\eta}_{rr}/\tilde{\eta}_{\theta\theta}) \\ \cot\theta \\ 0 \\ \tilde{h}_z + (2/r)(\tilde{\eta}_{rz}/\tilde{\eta}_{\theta\theta}) \end{pmatrix}. \quad (3)$$

The coordinate conditions are now imposed via the $\tilde{h}_\mu$. The $\tilde{\eta}_{\mu\nu}$, $\tilde{W}$, and $\tilde{h}_\mu$ constitute the full set of fundamental variables in our simulations.

The brane imposes interesting new physics, as well as new challenges for numerical calculations. During the evolutions, while the damping term introduced in Ref. [15] suffices to damp the constraint-violating modes in the bulk, it cannot control the corresponding modes appearing at and near the brane. We solve this problem by explicitly enforcing the constraints at the brane. These constraints can be converted into conditions on $\tilde{\eta}_{\mu z,z}|_{z=\ell}$, and can therefore be treated as boundary conditions. Generically there are no boundary conditions for $\tilde{\eta}_{\mu z}$ [13] at the brane, but by utilizing the coordinate freedom there we impose the additional boundary conditions $\tilde{\eta}_{tz}|_{z=\ell} = \tilde{\eta}_{rz}|_{z=\ell} = 0$, so that apparent horizons and the brane are perpendicular where they intersect [16].

Results.—Our scheme can be used to study a wide range of dynamical processes, but here we focus attention on the end states of gravitational collapse. Our expectation is that these end states will be stationary and, as will be seen, there is fairly strong evidence that this is the case. Our initial data for the massless scalar field on the brane, $z = \ell$, are a localized Gaussian pulse, given by $\Phi(0, r) = A_0 \exp[-(r - x_0)^2/\sigma_r^2]$, where A_0, x_0, and σ_r are adjustable parameters. We further specify the initial data to be time symmetric, so the pulse evolves into distinct ingoing and outgoing pieces. For weak data, and completely analogously to the four-dimensional GR case, the ingoing pulse implodes through $r = 0$, then propagates outwards to infinity (Fig. 1, left-hand panel). For strong enough initial data, on the other hand, the ingoing pulse becomes sufficiently self-gravitating that an apparent horizon with finite extension into the bulk forms (Fig. 1, right-hand panel). We use this as a signal that the resulting spacetime contains a black hole, also with finite extension into the bulk. Once an apparent horizon is detected in a calculation, we implement black hole

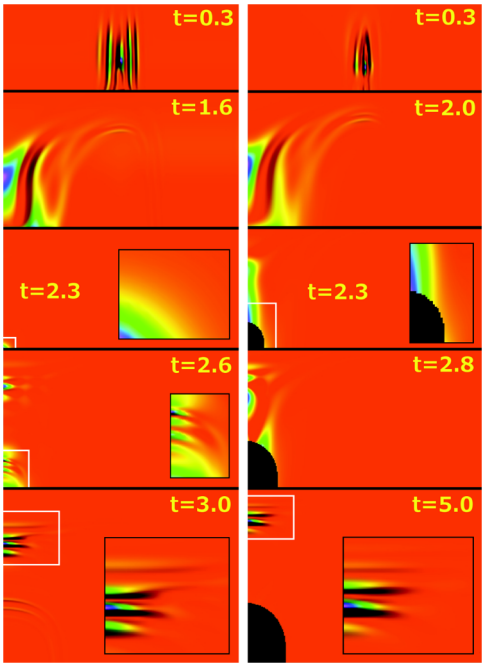

FIG. 1. Time evolution of the Kretschmann scalar $R_{\mu\nu\alpha\beta}R^{\mu\nu\alpha\beta}$ from two calculations with initial data having parameters $(A_0, x_0, \sigma_r) = (0.04, 2, 0.2)$ (left-hand panel) and (0.24,2,0.2) (right-hand panel), respectively. Evolution proceeds top to bottom. The time label is coordinate time t, and the horizontal and vertical axes are the compactified computational coordinates $\hat{R}$ and $\hat{Z}$ with compactification parameters $(r_0, z_0) = (2, 2)$, so that the bottom of each panel is $z = \ell$. The evolution on the left results in complete dispersal of the scalar field, while that on the right generates a black hole with $r_a = 0.61\ell$. The black ellipses in the bottom three frames of the right-hand sequence are regions interior to apparent horizons. The insets (outlined in black) are magnified views of portions of the corresponding frames (outlined in white) and are designed to highlight various features of the calculations.

excision [17], which enables us to continue the evolution for many dynamical times.

Our main analysis of the features of the black holes that form is made through the structure of the apparent horizons in the bulk. As is well known, the apparent horizon does not generally coincide with the event horizon. However, if an apparent horizon exists in a stationary, regular predictable spacetime, it does agree with the event horizon [4]. Furthermore, when there is no matter in the vicinity of a horizon, the intersection of the bulk event horizon with the brane can be shown to be a well-defined event horizon on the brane [18]. Since our spacetimes are axisymmetric, the intersection of an apparent horizon with the brane is spherically symmetric on the brane, and the intersection's proper area $\mathcal{A}_{\rm brane}$ defines an areal radius, $r_a \equiv \sqrt{\mathcal{A}_{\rm brane}/4\pi}$, which is called the *size* of the black hole [6]. During the calculations we monitor r_a as well as the proper area of the horizon in the bulk $\mathcal{A}_{\rm bulk}$ and the proper circumference of the horizon extended into the bulk C_5.

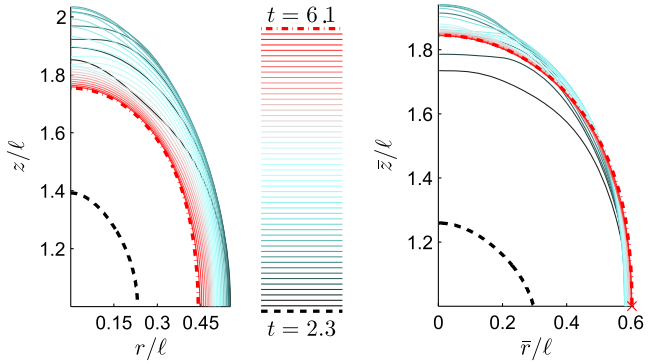

FIG. 2. Evolution of the apparent horizon for initial conditions $(A_0, x_0, \sigma_r) = (0.24, 2, 0.2)$. The left-hand panel shows the evolution in coordinate space (r, z), while the right-hand panel shows the time development of the apparent horizons in the background space whose coordinates are denoted $(\bar{r}, \bar{z})$, and where the embedding of the horizons in the background preserves their intrinsic geometries. The middle panel defines the legend for the line colors and line types. The black dashed line denotes the first apparent horizon which appeared at $t = 2.3$, while the red dot-dashed line is the last horizon computed at $t = 6.1$. Intermediate horizons are represented by lines with colors changing continuously from black to red as the evolution progresses. The embedding graph (right-hand panel) shows that the apparent horizons converge to a limiting line, which represents the physical process of the black hole settling into an apparently stationary state. The intersection of the brane with the horizon corresponding to this state is marked with an $\times$ in the graph (lower right). From the definition of r_a, the coordinates of the intersection are $(\bar{r}, \bar{z}) = (r_a, \ell)$.

To further analyze the apparent horizons, we generate embedding diagrams in the background space that preserve the intrinsic geometries of the horizons [13]. Figure 2 shows sample time developments of the apparent horizon displayed both in coordinate space and using embedding diagrams, for the same calculation visualized in the right-hand panel of Fig. 1.

We are interested in the long-term behavior of the black hole solutions and, in particular, the extent to which stationary end states are achieved. If the slicing condition is such that the $t = \text{const}$ slices are Lie dragged by the Killing vector associated with the putatively stationary end state, the intrinsic geometry of the apparent horizon will itself be time independent, resulting in a stationary embedding plot. Unfortunately, such a slicing condition is nontrivial to devise and we have yet to formulate one. However, during a typical long-term evolution of a collapsing configuration, where the elapsed integration time is much greater than the characteristic dynamical time scale, we find that the solution settles into some apparently stationary state that we use to approximate the true end state. We note that the evolution inevitably departs from this configuration. We assume that this is a coordinate effect but have not yet been able to develop a technique to show that this is the case. Operationally we identify the apparently stationary

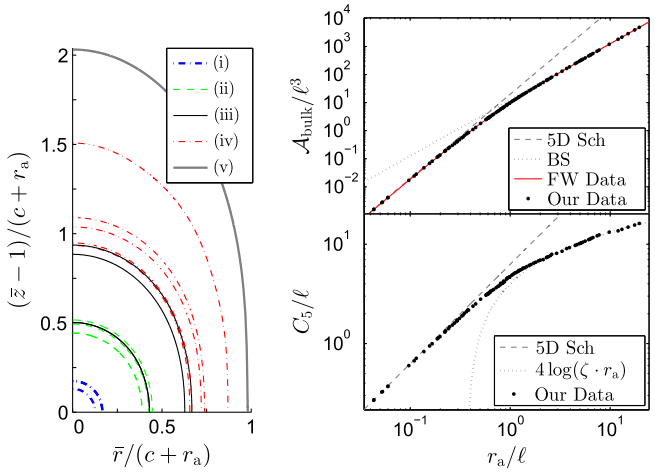

FIG. 3. Left: Apparently stationary black holes generated from different initial data families, visualized using the embedding of apparent horizons in the background space whose coordinates are $(\bar{r},\bar{z})$, and where the compactification parameter is $c=0.3\ell$. This plot provides evidence that the black holes generated from distinct initial data families form a single, unique sequence. Additionally, the sequence appears to be "monotonic" in the sense that for initial data strengths A_0 and A_0', where $A_0{}'>A_0$, the horizon embedding curve for A_0' lies entirely outside of that for A_0. Three black holes from family (iii) are shown here; the smallest fits precisely between the two largest of family (ii), while the largest is well fit by the smallest of family (iv). Upper right: $\mathcal{A}_{\rm bulk}$ as a function of r_a, with a comparison with the data obtained by Figueras and Wiseman (FW) [6]. Small black holes asymptote to their five-dimensional Schwarzschild (5D Sch) counterparts and the $\mathcal{A}_{\rm bulk}$-versus-r_a relation of large black holes asymptotes to that of black strings (BS). Lower right: C_5 as a function of r_a.

states by looking for approximate time independence in the embedding diagrams, as illustrated in the right-hand panel of Fig. 2.

We have performed a series of evolutions using five distinct initial data families, from which we have obtained black holes with sizes in the range $0.04\ell \lesssim r_a \lesssim 19.6\ell$. Within each family only A_0 is varied; x_0 and σ_r are held fixed. The specific values of (x_0,σ_r) for the families are (i) (0.5,0.1), (ii) (1,0.1), (iii) (2,0.2), (iv) (0,0.3), and (v) (2,0.5). The apparently stationary states for the complete set of evolutions are plotted in the left-hand panel of Fig. 3, where the axes have been scaled in order to accommodate the significant range of sizes of the black holes. The figure shows preliminary evidence that the specific black holes in the RSII spacetimes studied here—which are axisymmetric in the bulk, and which have no angular momentum or nongravitational charges—comprise a unique sequence, regardless of the details of the initial data. Furthermore, since the sequence is monotonic in the sense defined in the figure caption, we can use r_a to define the position of any given black hole in the sequence. If the black hole solutions are unique, the black holes we obtain from dynamical evolution should agree with those previously obtained via a static vacuum ansatz by Figueras and Wiseman [6,7]. The comparison with their results is shown in the upper right-hand panel of Fig. 3, which plots $\mathcal{A}_{\rm bulk}$ as a function of r_a. Clearly the agreement is very good.

When the sizes of the black holes are much smaller than ℓ, the solutions tend to five-dimensional asymptotically flat Schwarzschild ones [6]. As shown in the left-hand panel of Fig. 3, as the size of the black hole increases, its embedding-diagram shape changes from spherical to prolate (cigar shaped). Now, large black holes have an upper limit, which is the corresponding $\mathrm{AdS}_5/\mathrm{CFT}_4$ solution [6,13]. The geometry of the portion of a large black hole that is close to the brane behaves like that of a black string, which makes the $\mathcal{A}_{\rm bulk}$-versus-r_a relation gradually change into that of black strings. To study the difference between large black holes and black strings, we plot C_5 versus r_a in the lower right-hand panel of Fig. 3. Again, we see that small black holes are asymptotically five-dimensional Schwarzschild, so $C_5 \sim 2\pi r_a$. For large black holes, C_5 is well approximated by $C_5 \sim 4\log(\zeta\cdot r_a)$ [19], as long as the *shape* of the holes (as seen in an embedding plot) does not change with the size [13]. For our data we find a best fit $\zeta \approx 2.71$ while Figueras and Wiseman [19] independently and previously obtained $\zeta \approx 2.8$ from their static vacuum calculations. The proper circumference C_5 increases with r_a, but the ratio C_5/r_a shrinks as $\sim \log r_a/r_a$. Therefore, large black holes are actually prolate (flattened pancakes) as determined from their intrinsic geometry. This was first suggested in Ref. [20].

Conclusion and discussion.—We have performed the first numerical study of the full dynamics of a braneworld within the framework of the RSII model. We find that the result of gravitational collapse of a strong pulse of massless scalar field is a black hole with finite extension into the bulk. There is preliminary evidence that the black holes that form constitute a unique sequence that can be conveniently parametrized by the areal radius of the horizon. Additionally, the black hole solutions that we compute have properties in agreement with those found previously from a static vacuum ansatz [6,7].

Our approach could be improved through the development of a slicing condition that would adapt to the assumed time translational symmetry of the stationary end states. Black holes with size $0.04\ell \lesssim r_a \lesssim 19.6\ell$ were constructed here. Consideration of a wider range of sizes would also require improvement of coordinate conditions. It would be particularly useful to be able to probe the regime of small black holes since the nature of black hole critical phenomena in this scenario could well be different than it is in usual four-dimensional spacetime.

This research was supported by NSERC and CIFAR. We thank Evgeny Sorkin and William Unruh for useful discussions, and Toby Wiseman and Pau Figueras for providing their data and discussing it with us. Some of the calculations were performed using the Westgrid facilities of Compute Canada.

[1] L. Randall and R. Sundrum, Phys. Rev. Lett. **83**, 3370 (1999); **83**, 4690 (1999).
[2] T. Shiromizu, K. I. Maeda, and M. Sasaki, Phys. Rev. D **62**, 024012 (2000).
[3] A. Chamblin, S. W. Hawking, and H. S. Reall, Phys. Rev. D **61**, 065007 (2000).
[4] S. W. Hawking and G. F. R. Ellis, *The Large Scale Structure of Space-Time*, Cambridge Monographs on Mathematical Physics (Cambridge University Press, Cambridge, England, 1973).
[5] R. Gregory and R. Laflamme, Phys. Rev. Lett. **70**, 2837 (1993); R. Gregory, Classical Quantum Gravity **17**, L125 (2000).
[6] P. Figueras and T. Wiseman, Phys. Rev. Lett. **107**, 081101 (2011).
[7] P. Figueras, Springer Proc. Math. Stat. **60**, 37 (2014).
[8] P. Figueras, J. Lucietti, and T. Wiseman, Classical Quantum Gravity **28**, 215018 (2011).
[9] S. Abdolrahimi, C. Cattoen, D. N. Page, and S. Yaghoobpour-Tari, Phys. Lett. B **720**, 405 (2013).
[10] W. Israel, Nuovo Cimento **44**, 1 (1966).
[11] F. Pretorius, Classical Quantum Gravity **22**, 425 (2005).
[12] R. M. Wald, *General Relativity* (The University of Chicago Press, Chicago, 1984).
[13] D. Wang, Ph. D. thesis, The University of British Columbia, 2015, arXiv:1505.00093.
[14] M. Ruiz, M. Alcubierre, and D. Nunez, Gen. Relativ. Gravit. **40**, 159 (2008).
[15] C. Gundlach, J. M. Martin-Garcia, G. Calabrese, and I. Hinder, Classical Quantum Gravity **22**, 3767 (2005).
[16] W. G. Unruh and R. M. Wald (private communication).
[17] W. G. Unruh (private communication).
[18] H. Ishihara, Phys. Rev. Lett. **86**, 381 (2001).
[19] P. Figueras and T. Wiseman (private communication).
[20] S. B. Giddings, E. Katz, and L. Randall, J. High Energy Phys. 03 (2000) 023.